JACS
JOURNAL OF THE AMERICAN CHEMICAL SOCIETY

Communication

pubs.acs.org/JACS

Controlling the Intercalation Chemistry to Design High-Performance Dual-Salt Hybrid Rechargeable Batteries

Jae-Hyun Cho,[†,‡,∥] Muratahan Aykol,[§,∥] Soo Kim,[§,∥] Jung-Hoon Ha,[†] C. Wolverton,*[,§] Kyung Yoon Chung,*[,†] Kwang-Bum Kim,[‡] and Byung-Won Cho[†]

[†]Center for Energy Convergence Research, Korea Institute of Science and Technology, Hwarang-ro 14-gil 5, Seongbuk-gu, Seoul 136-791, Republic of Korea

[‡]Department of Materials Science and Engineering, Yonsei University, 50 Yonsei-ro, Seodaemun-gu, Seoul 120-749, Republic of Korea

[§]Department of Materials Science and Engineering, Northwestern University, 2220 Campus Drive, Evanston, Illinois 60208, United States

Supporting Information

ABSTRACT: We have conducted extensive theoretical and experimental investigations to unravel the origin of the electrochemical properties of hybrid Mg^{2+}/Li^+ rechargeable batteries at the atomistic and macroscopic levels. By revealing the thermodynamics of Mg^{2+} and Li^+ co-insertion into the Mo_6S_8 cathode host using density functional theory calculations, we show that there is a threshold Li^+ activity for the pristine Mo_6S_8 cathode to prefer lithiation instead of magnesiation. By precisely controlling the insertion chemistry using a dual-salt electrolyte, we have enabled ultrafast discharge of our battery by achieving 93.6% capacity retention at 20 C and 87.5% at 30 C, respectively, at room temperature.

Rechargeable magnesium batteries are emerging as a possible new class of energy storage systems beyond the conventional lithium-ion technology.[1−13] Unlike the Li metal, Mg replating does not lead to dendrite formation,[6,14] and therefore, a Mg anode provides very high capacity and energy density[15] with no compromise in safety, at a significantly lower cost compared to Li.[6] Chevrel phases (CPs) have been of particular interest for the discovery of novel secondary batteries other than Li-ion, as they allow fast and reversible insertion of various mono- and multivalent cations.[1,2,16] The first prototype of rechargeable magnesium batteries was in fact introduced more than a decade ago using the CP-type Mo_6S_8 as the cathode material.[3] In these Mg-Mo_6S_8 batteries, two Mg^{2+} ions per formula unit can be inserted into the Mo_6S_8 host, each ion leading to a distinct voltage plateau upon discharge, with a total theoretical capacity of 122 mAh g^{-1}. The first of these Mg^{2+} ions is known to occupy the "inner ring" (A) sites of the host material,[2,4] where it becomes kinetically trapped at room temperature.[5] Consequently, the resulting capacity drops below 80 mAh g^{-1}, and the battery can cycle mainly by Mg^{2+} insertion to the lower potential "outer ring" (B) sites. Hence, to reach their theoretical capacities these batteries require elevated temperature operation to overcome the sluggish Mg^{2+} transport in Mo_6S_8, despite the inherently open structure of this cathode material.[1,2,4,5] In contrast, fast ionic transport in the entire intercalation range was reported for Ni^{2+}, Zn^{2+}, and Li^+ in CPs.[1] Among these ions, only Li^+ has a lower standard reduction potential than Mg^{2+}, and can reach higher voltages than the Mg counterpart. If crafted carefully, therefore, a hybrid Mg/Li-ion battery can synergistically exploit the advantages of Mg- and Li-Mo_6S_8 systems. While such designs were hypothesized in past[7] and Mg/Li dual-salt batteries with a $LiFePO_4$ cathode[15] and a Mo_6S_8 cathode[17,18] have been tested in very recent studies, the underlying mechanisms have not been fully revealed in detail. Here, we present a novel theory-aided framework to design dual-salt Mg^{2+}/Li^+ batteries by controlling the Mg^{2+} and Li^+ insertion chemistry at the cathode via tuning the Li^+ activity in the electrolyte and by ensuring that Mg plating/dissolution (Mg/Mg^{2+}) is the sole reaction at the anode at all times. This approach has allowed us to design the hybrid Mg^{2+}/Li^+ rechargeable battery with an all-phenyl complex (APC) 0.2 M and lithium chloride (LiCl) 0.5 M electrolyte, which can discharge in as fast as 2 min with remarkable capacity retention. Our results suggest an avenue for chemically designing safe and cost-effective dual-salt systems.

We first examine the thermodynamics underlying the (co)-insertion of Mg^{2+} and Li^+ into the Mo_6S_8 cathode by calculating the stabilities of ionic configurations with density functional theory (DFT) as shown in Figure 1. It is possible to insert up to four Li^+ or two Mg^{2+} ions, or different co-insertion arrangements that lead to transfer of four electrons per Mo_6S_8.[19] Mg^{2+} or Li^+ insertion at the cathode at any stage of discharge can be described with the following reaction:

$$XMo_6S_8 + xM^{n+} + nxe^- \rightarrow M_xXMo_6S_8 \quad (1)$$

where M^{n+} can be Mg^{2+} or Li^+, and X denotes the host ions that were already inserted prior to this reaction. Reactions in Figure 1 are labeled as inserting-ion/host-ions, i.e., M_x/X. For example, Mg_1/Li_1 denotes the cathode reaction $LiMo_6S_8 + Mg^{2+} + 2e^- \rightarrow MgLiMo_6S_8$ and Li_2/Li_1 denotes the cathode reaction $LiMo_6S_8 + 2Li^+ + 2e^- \rightarrow Li_3Mo_6S_8$. Mg_1 and Li_1 denote initial reactions of Mg^{2+} or Li^+ insertion into the pristine Mo_6S_8 electrode. We consider three distinct groups of crystallographic sites that Mg^{2+} and Li^+ can occupy in Mo_6S_8 based on the previous experimental and DFT analysis[2] and the crystal structure of $Li_4Mo_6S_8$.[16,20] These sites are illustrated schematically in Figure 1. Our DFT

Received: August 18, 2014
Published: November 3, 2014

   dx.doi.org/10.1021/ja508463z | J. Am. Chem. Soc. 2014, 136, 16116−16119

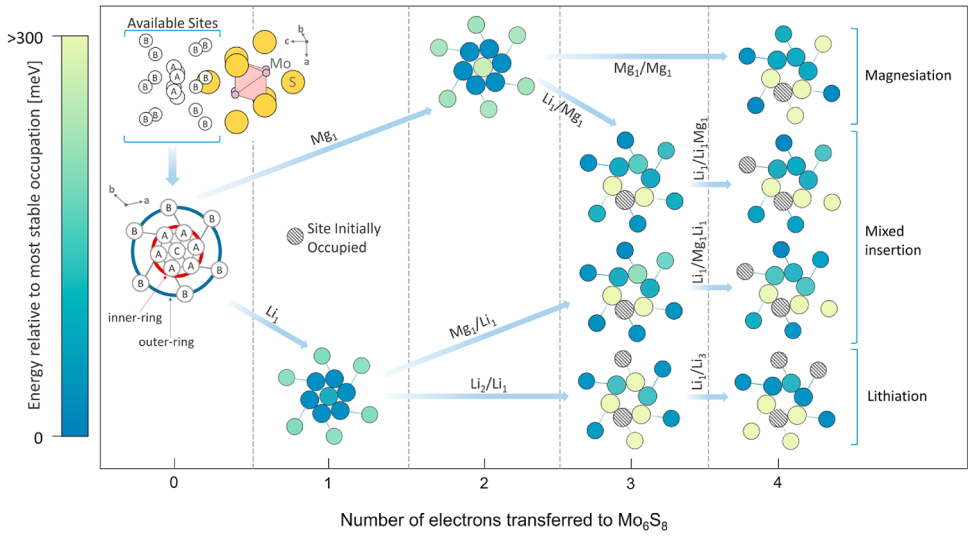

Figure 1. Energetic stabilities of the occupations of available interstitial sites in Mo_6S_8 by Mg^{2+} and Li^+ along various Mg^{2+}/Li^+ (mixed)-insertion paths calculated by DFT. Available sites considered (A–C) are shown schematically. The lowest energy configuration corresponds to zero on the given energy scale, and all sites (represented as circles) are colored based on their occupation energy relative to this lowest energy configuration. Sites that are already occupied during insertion are shown as hatched circles. Arrows indicate possible reaction paths, and schematics do not reflect the distortions of actual site positions.

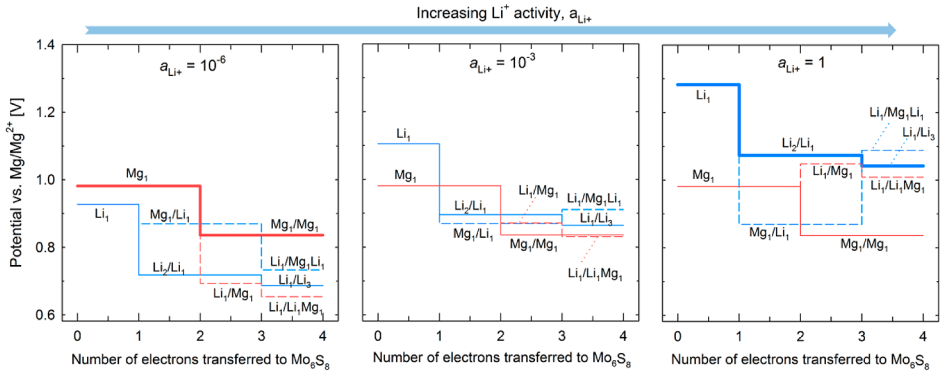

Figure 2. Lithiation and magnesiation potentials of Mo_6S_8 (vs Mg/Mg^{2+}) at different Li^+ activities (a_{Li+}) determined by combining DFT energies with the Nernst equation. Mixed-insertion paths where Li^+ and Mg^{2+} occupy different sites in the same Mo_6S_8 host are shown as dashed lines. Full magnesiation and full lithiation paths are shown in bold.

calculations (Supporting Information, SI) demonstrate that regardless of its chemical identity, the first ion inserted into the Mo_6S_8 primitive cell always energetically prefers to occupy the A sites, which is consistent with previous studies.[2,16] Subsequently inserted Mg^{2+} or Li^+ ions energetically prefer to occupy B sites, but arrangements of ions and relative stabilities of occupations vary depending on the insertion path as described in Figure 1.

Having determined the relative energetic stabilities of ionic configurations in Mo_6S_8 at multiple stages of discharge in Figure 1, we calculate the equilibrium cell potentials vs Mg/Mg^{2+} as a function of Li^+ activity, by combining DFT energies with the Nernst eq (SI). The calculated hybrid Mg^{2+}/Li^+ full cell potentials are shown in Figure 2. Our predicted Mg_1 voltage is in good agreement with experiments[1−12] (closer to experiment than a previous calculation)[21] and agrees well with a recent hybrid-functional calculation.[22] In Figure 2, with the Mg metal anode, lithiation and magnesiation of the Mo_6S_8 cathode both yield comparable voltages. Therefore, the insertion chemistry at the cathode strongly depends on the Li^+ activity in the electrolyte as shown in Figure 2. In cells with low initial Li^+ activities (e.g., $a_{Li+} = 10^{-6}$), we find that the Mo_6S_8 cathode is completely magnesiated. When the Li^+ activity is increased to $\sim 10^{-3}$, the lithiation voltage raises above magnesiation voltage for the first insertion step. Thus, there is a threshold Li^+ activity for the pristine Mo_6S_8 cathode to initially prefer lithiation of A sites instead of magnesiation. However, since Li^+ activity in the electrolyte will decrease during discharge, this initial lithiation may switch to magnesiation before reaching one Li^+ per Mo_6S_8 formula unit. In that case, a two-step co-intercalation path closer to Mg_1/Li_1 and Li_1/Mg_1Li_1 may follow the first discharge step. Even if A sites can be completely lithiated, Mg^{2+} and Li^+ insertion potentials for the subsequent steps are still so close that co-insertion can occur in those steps. Hence, to suppress magnesiation completely and reach full lithiation up to $Li_4Mo_6S_8$, Li^+ activity in the electrolyte must be further increased close to unity.

While Li^+ and Mg^{2+} insertion can both take place at the cathode, the concept relies on that Li^+ does not participate in the anodic reaction. Although Li/Li^+ requires a ~0.68 V overpotential to occur instead of Mg/Mg^{2+} while charging the battery (estimated based on standard electrode potentials[23]), this

dx.doi.org/10.1021/ja508463z | J. Am. Chem. Soc. 2014, 136, 16116−16119

potential difference can vanish if Mg-Li alloying is energetically favorable. Alloying reaction of Li^+ with the Mg electrode can be written as

$$Li^+ + e^- \rightarrow \underline{Li}^{Li_xMg_{1-x}} \quad (2)$$

where $\underline{Li}^{Li_x\,Mg_{1-x}}$ denotes Li in $Li_x\,Mg_{1-x}$ alloy at a composition x. Using experimental thermochemical data (See SI), we calculate the corresponding half-cell potential ($\varepsilon_{Li_x\,Mg_{1-x}}$) as a function of x (Figure 3), for different Li^+ activities in the electrolyte. We find

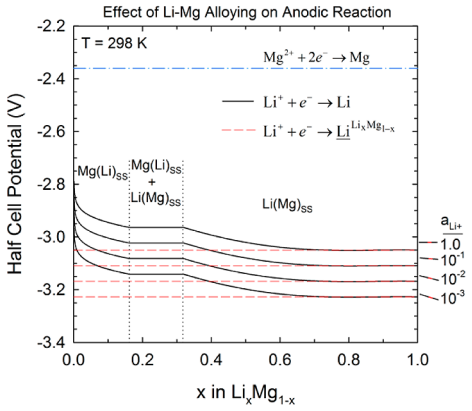

Figure 3. Potential for the Li-Mg alloying anode half-reaction as a function of x and Li^+ activity. The alloying reaction is $Li^+ + e^- \rightarrow \underline{Li}^{Li_xMg_{1-x}}$, where $\underline{Li}^{Li_xMg_{1-x}}$ denotes Li in Li_xMg_{1-x}. Alloying results in a deviation from the corresponding $Li^+ + e^- \rightarrow Li$ potentials for any given Li^+ activity. Even with Li-Mg alloying, however, lithiation potentials cannot reach that of $Mg^{2+} + 2e^- \rightarrow Mg$ at any x. Potential is given with respect to standard hydrogen electrode (T = 298 K).

that for any practical Li^+ activity, $\varepsilon_{Li_x\,Mg_{1-x}}$ remains below $\varepsilon^0_{Mg^{2+}}$ at all x, because the work required to reduce the Li ions exceeds the free-energy gain acquired from the Mg-Li alloy formation. Thus, the Mg-Li alloy electrodeposition cannot occur above the Mg redox potential.

Based on the theoretical guidelines above, we can now control the insertion chemistry solely at the cathode, and subsequently the discharge potential of the hybrid cell by varying the LiCl content of the electrolyte. In Figure 4a, we show that when the electrolyte contains only 0.4 M APC, the battery operates completely by Mg^{2+} insertion into Mo_6S_8. Despite the appearance of the two characteristic plateaus at 1.21 and 1.10 V, the discharge capacity is limited to 83.0 mAh g^{-1} at room temperature. The rate capability is poor, and only half of the theoretical capacity is utilizable at a 1 C rate (Figure 4b). When we add LiCl to the system to tailor the insertion chemistry, fast Li^+ insertion to the A sites is immediately observed from the distinct plateaus that appear at a higher voltage region (~1.6–1.7 V) corresponding to an initial lithiation in Figure 4a. The amount of Li^+ insertion in this step is proportional to the LiCl concentration. Furthermore, the capacity from this initial lithiation step clearly accounts for a significant portion of the overall capacity gain of each sample with respect to the pure Mg battery. As is evident from the DFT calculations in Figure 2, the voltages of the initial lithiation steps (Li_1) rise with increasing LiCl content due to the increasing Li^+ activities. For very low LiCl contents, A sites can be further magnesiated after the initial lithiation due to decreasing Li^+ activity upon discharge (e.g., transition from a_{Li+} of 10^{-3} to 10^{-6} in Figure 2), followed mainly by magnesiation of B sites. This three stage discharge behavior is consistent with the discharge profile of the sample with 0.05 M LiCl in Figure 4a. As we further increase the LiCl concentration, the discharge curves start to exhibit a two-stage-like profile, and a slight increase in the voltage of the second plateau is observed in Figure 4a. The voltage increase can be partially explained by the slightly higher insertion potential of Mg^{2+} to B sites in samples with Li^+ on A sites compared to that with Mg^{2+} on A sites (Mg_1/Li_1 vs Mg_1/Mg_1 in Figure 2). However, the smooth profiles after the initial step are likely to be

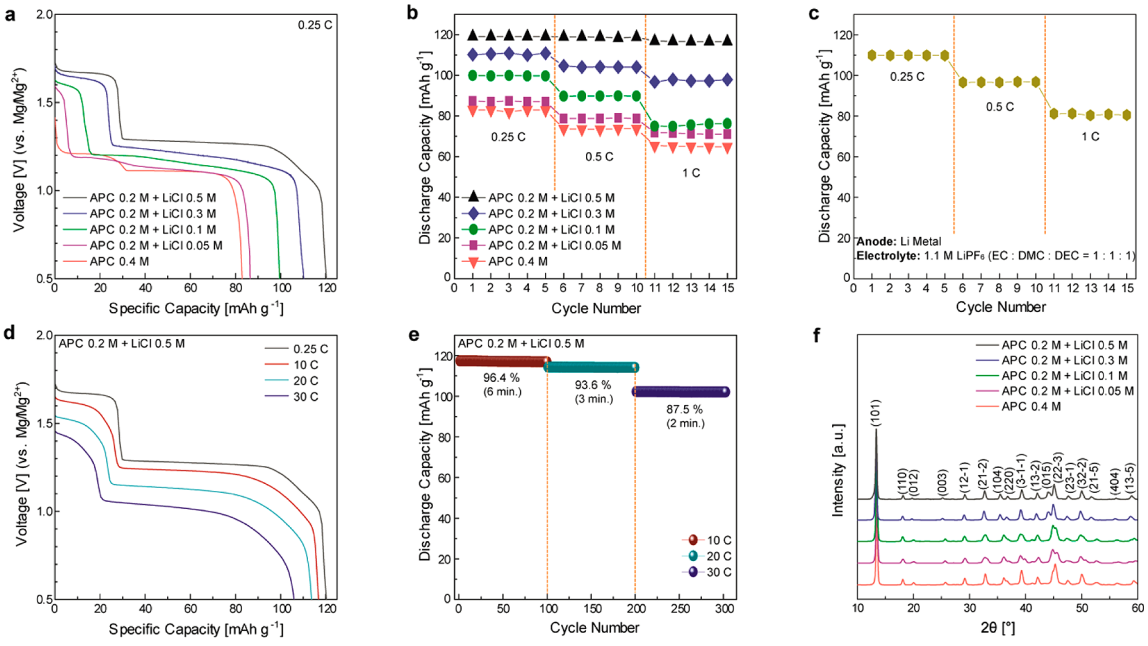

Figure 4. (a) Discharge profiles at varying LiCl concentrations. Rate capabilities of (b) Mg^{2+}/Li^+ hybrid battery as a function of LiCl content and (c) a Li metal anode-Mo_6S_8 cathode battery with $LiPF_6$-based electrolyte. (d) Discharge profiles of the hybrid battery with the APC 0.2 M + LiCl 0.5 M electrolyte at high rates. (e) Cycle characteristics of the hybrid rechargeable battery shown in (d). (f) *Ex situ* XRD patterns of completely discharged cathode materials. Electrochemical data provided in (a–e) are achieved after the formation cycle of the cell activation process (SI).

dx.doi.org/10.1021/ja508463z | J. Am. Chem. Soc. 2014, 136, 16116–16119

a result of mixed intercalation due to lithiation and magnesiation potentials becoming very close in intermediate Li^+ activity levels (e.g., a_{Li+} of 10^{-3} in Figure 2). Transition from a magnesiating to lithiating cathode with increasing Li^+ activity is further signaled by the changes in the separations of adjacent peaks in the *ex situ* X-ray diffraction (XRD) patterns of in Figure 4f, such as (104) and (220) near 36° or (015) and (22−3) near 45°. As we increase the LiCl concentration, patterns shift to lower angles, and unit-cell volume of the cathode monotonically increases (Table S1). Since the insertion of two Li^+ ions transfers the same charge as one Mg^{2+} ion and their ionic radii are similar, the expansion in the fully discharged unit-cell volume is a clear indication of an increase in lithiation over magnesiation. This trend is further supported by elemental mapping (Figure S5).

For the samples with LiCl content ≤0.3 M, discharge capacity is still sensitive to the current rate in Figure 4b, which means any remnant magnesiation still plays a role in hampering the rate capability. DFT voltages in Figure 2 indicate that we must sustain higher Li^+ activities to ensure that both Li_2/Li_1 and Li_1/Li_3 are thermodynamically more favorable than Mg^{2+} and Li^+ co-intercalation. By increasing the LiCl concentration to 0.5 M in the APC electrolyte, we accordingly find that almost the full theoretical capacity of $Li_4Mo_6S_8$ can be achieved with an excellent rate capability at room temperature. At 0.25 C, first lithium enters the cathode at 1.66 V, and Li_2/Li_1 insertion occurs at 1.28 V followed by the insertion of fourth Li at a decreasing potential in Figure 4a. The rate capability of this hybrid Mg^{2+}/Li^+ rechargeable battery with APC 0.2 M and LiCl 0.5 M electrolyte is superior compared to all other electrolyte concentrations as shown in Figure 4b. There is almost no drop in the discharge capacity up to 1 C discharging rate for the hybrid system. In comparison, the Li anode-Mo_6S_8 cathode system loses capacity at higher rates (Figure 4c). The theory-aided design of the hybrid system allows exceptionally fast discharge rates and delivers 96.4% of theoretical capacity at 10 C, 93.6% at 20 C, and 87.5% at 30 C (Figure 4d,e).

A challenge that these dual-salt systems face is that the active ions need to be stored in the electrolyte.[15] Although the low density of ions in the liquid electrolyte will result in a penalty in energy density, other factors, such as using a metal anode, as well as the increase in voltage and capacity will result in an increase in the energy density. Future work is certainly required to more fully take advantage of these promising aspects of the hybrid Mg^{2+}/Li^+ battery technology. Our combined computational/experimental approach paves the way for the development of new hybrid batteries with controlled intercalation chemistry.

■ ASSOCIATED CONTENT

Ⓢ Supporting Information

Experimental & computational methods and data. This material is available free of charge via the Internet at http://pubs.acs.org.

■ AUTHOR INFORMATION

Corresponding Authors

c-wolverton@northwestern.edu
kychung@kist.re.kr

Author Contributions

‖These authors contributed equally.

Notes

The authors declare no competing financial interest.

■ ACKNOWLEDGMENTS

S.K. was supported by the Northwestern-Argonne Institute of Science and Engineering (NAISE). M.A. and C.W. were supported by The Dow Chemical Company. J.C., K.C., and B.C. were partially supported by the Energy Efficiency & Resources of the Korea Institute of Energy Technology Evaluation and Planning (Project No. 20112010100140) grant funded by the Korea government Ministry of Trade, Industry & Energy. J.C., J.H., K.C., K.K., and B.C. were supported by the KIST Institutional Program (Project No. 2E24663). The authors would like to thank Jae-Kyo Noh and Haesik Kim for the EDX and XRD measurements.

■ REFERENCES

(1) Levi, E.; Gershinsky, G.; Aurbach, D.; Isnard, O.; Ceder, G. *Chem. Mater.* **2009**, *21*, 1390.
(2) Levi, E.; Lancry, E.; Mitelman, A.; Aurbach, D.; Ceder, G.; Morgan, D.; Isnard, O. *Chem. Mater.* **2006**, *18*, 5492.
(3) Aurbach, D.; Lu, Z.; Schechter, A.; Gofer, Y.; Gizbar, H.; Turgeman, R.; Cohen, Y.; Moshkovich, M.; Levi, E. *Nature* **2000**, *407*, 724.
(4) Levi, E.; Lancry, E.; Mitelman, A.; Aurbach, D.; Isnard, O.; Djurado, D. *Chem. Mater.* **2006**, *18*, 3705.
(5) Levi, M. D.; Lancry, E.; Gizbar, H.; Lu, Z.; Levi, E.; Gofer, Y.; Aurbach, D. *J. Electrochem. Soc.* **2004**, *151*, A1044.
(6) Muldoon, J.; Bucur, C. B.; Oliver, A. G.; Sugimoto, T.; Matsui, M.; Kim, H. S.; Allred, G. D.; Zajicek, J.; Kotani, Y. *Energy Environ. Sci.* **2012**, *5*, 5941.
(7) Gofer, Y.; Chusid, O.; Gizbar, H.; Viestfrid, Y.; Gottlieb, H. E.; Marks, V.; Aurbach, D. *Electrochem. Solid-State Lett.* **2006**, *9*, A257.
(8) Lancry, E.; Levi, E.; Gofer, Y.; Levi, M.; Salitra, G.; Aurbach, D. *Chem. Mater.* **2004**, *16*, 2832.
(9) Mizrahi, O.; Amir, N.; Pollak, E.; Chusid, O.; Marks, V.; Gottlieb, H.; Larush, L.; Zinigrad, E.; Aurbach, D. *J. Electrochem. Soc.* **2008**, *155*, A103.
(10) Aurbach, D.; Weissman, I.; Gofer, Y.; Levi, E. *Chem. Rec.* **2003**, *3*, 61.
(11) Levi, E.; Mitelman, A.; Aurbach, D.; Brunelli, M. *Chem. Mater.* **2007**, *19*, 5131.
(12) Lancry, E.; Levi, E.; Mitelman, A.; Malovany, S.; Aurbach, D. *J. Solid State Chem.* **2006**, *179*, 1879.
(13) Ichitsubo, T.; Yagi, S.; Nakamura, R.; Ichikawa, Y.; Okamoto, S.; Sugimura, K.; Kawaguchi, T.; Kitada, A.; Oishi, M.; Doi, T.; Matsubara, E. *J. Mater. Chem. A* **2014**, *2*, 14858.
(14) Matsui, M. *J. Power Sources* **2011**, *196*, 7048.
(15) Yagi, S.; Ichitsubo, T.; Shirai, Y.; Yanai, S.; Doi, T.; Murase, K.; Matsubara, E. *J. Mater. Chem. A* **2014**, *2*, 1144.
(16) Ritter, C.; Gocke, E.; Fischer, C.; Schöllhorn, R. *Mater. Res. Bull.* **1992**, *27*, 1217.
(17) Cheng, Y.; Shao, Y.; Zhang, J.-G.; Sprenkle, V. L.; Liu, J.; Li, G. *Chem. Commun.* **2014**, *50*, 9644.
(18) Mohtadi, R.; Matsui, M.; Arthur, T. S.; Hwang, S.-J. *Angew. Chem., Int. Ed.* **2012**, *51*, 9780.
(19) Gocke, E.; Schollhorn, R.; Aselmann, G.; Muller-Warmuth, W. *Inorg. Chem.* **1987**, *26*, 1805.
(20) McKinnon, W. R.; Dahn, J. R. *Phys. Rev. B* **1985**, *31*, 3084.
(21) Kganyago, K. R.; Ngoepe, P. E.; Catlow, C. R. A. *Phys. Rev. B* **2003**, *67*, 104103.
(22) Kaewmaraya, T.; Ramzan, M.; Osorio-Guillén, J. M.; Ahuja, R. *Solid State Ionics* **2014**, *261*, 17.
(23) Bratsch, S. G. *J. Phys. Chem. Ref. Data* **1989**, *18*, 1.